Charge regulation of nanoparticles in the presence of multivalent electrolytes

Thiago Colla,[1] Amin Bakhshandeh,[2] and Yan Levin[2, a)]
[1)] *Instituto de Física, Universidade Federal de Ouro Preto, 35400-000, Ouro Preto, MG, Brazil*
[2)] *Instituto de Física, Universidade Federal do Rio Grande do Sul, Caixa Postal 15051, CEP 91501-970, Porto Alegre, RS, Brazil*

We explore charge regulation (CR) of spherical nanoparticles immersed in an asymmetric electrolyte of a specified pH. Using a recently developed reactive canonical Monte Carlo (MC) simulation method, titration isotherms are obtained for suspensions containing monovalent, divalent, and trivalent coions. A theory based on the modified Poisson-Boltzmann (PB) approximation, which incorporates the electrostatic ion solvation free energy and discrete surface charge effects, is used to compare with the simulation results. A remarkably good agreement is found without any fitting parameters, both for the ion distributions and titration curves, suggesting that ionic correlations between coions and hydronium ions at the nanoparticle surface play only a minor role in determining the association equilibrium between hydroniums and the functional sites on the nanoparticle surface. On the other hand, if suspension contains multivalent counterions, we observe large deviation between theory and simulations, showing that the electrostatic correlations between counterions and hydronium ions at the nanoparticle surface are very significant and must be properly taken into account to correctly describe CR for such solutions.

I. INTRODUCTION

Coulomb interactions are known to be the main driving force governing a wide range of important phenomena in physics[1,2], physical chemistry[3–6], biophysics[1,5,7–10] and material science[11,12]. Examples are abundant, ranging from the formation of macroscopic aggregates of suspended nanoparticles[13–16] to the cell functionality[8,17], DNA assembly and encapsulation in viruses[18–22], conformation of polyeletrolytes[9,23–25] and proteins[26–29], electric storage devices[30–32], sedimentation of charged colloids[33–39], etc. Controlling these interactions and understanding the role that they play in different phenomena is a mandatory step towards the development of new materials and advances in key applications in medicine, nanotechnology and biology[40]. The buildup of local charges that gives rise to such interactions is controlled by the local electrochemical equilibrium[1]. Typical examples are the formation of double-layer structures around charged surfaces, ion exchange through membranes, ion dissociation in polar media, and formation of covalent bonds between protons and acidic/basic groups on surfaces immersed in solvents.

Ion dissociation is a mechanism of entropic-electrostatic nature that occurs when neutral molecules are dissolved in a polar medium. The break up of ionic bond results in entropy gain from a counterion released into solution. In apolar medium, the entropic gain is not sufficient to compensate for the electrostatic penalty of exposing charge to a low dielectric environment[41,42]. On the other hand, in a strongly polar medium, such as water, the entropic gain can compensate the electrostatic self-energy penalty, resulting from breaking of ionic bonds[1,4,43,44]. Dissolving salt into an aqueous solution provides an efficient way of controlling electrostatic forces between charged surfaces, as the local electrochemical equilibrium results in partial screening of these interactions *via* formation of ion neutralizing clouds[45]. On the other hand, the charging mechanism of surfaces with weak acidic/basic groups also involves – in addition to entropic and electrostatic contributions – covalent bonding between protons and active surface groups[46,47]. For surfaces with acidic groups, considered in the present paper, proton exchange between donor and receptor molecules results in either charging (deprotonation) or neutralization (protonation) [48] of macromolecules. The important characteristic of this process is that the charge of a nanoparticle or a surface decorated with acid/base groups can be controlled by the amount of the acid/base added to the solution, *i. e.* the system's pH. Such controlling mechanism is generally referred to as the *Charge Regulation* (CR) mechanism[49–56]. The possibility of tuning the charge of nanoparticles by varying pH – alongside with the adjustment of the effective strength and range of Coulomb interactions by added salt – represents a convenient way of controlling the effective interactions between nanoparticles and surfaces in general[57–61]. As an example, the irreversible aggregation of particles such as charged colloidal suspensions subject to the gravitational field can be controlled by changing system's pH and the amount of added electrolyte[62–64].

Attempts to quantitatively describe the CR mechanism date back to the early 70's, with the pioneering work of Ninham and Parsegian (NP)[55]. The NP theory is based on the Poisson-Boltzmann (PB) mean-field description

[a)] Electronic mail: levin@if.ufrgs.br

of electrostatic interactions, with the adsorption of protons from solution controlled by the bulk acid dissociation constant[65]. NP theory does not account for the interfacial effects, as its formulation relies on the bulk equilibrium constant[55]. However, the equilibrium dissociation constants of acid can be quite different, depending if the residue is free in the bulk or bound to the surface[61,66–68]. Furthermore, it also ignores the electrostatic discrete surface charge effects[69], which have been shown to play a very important role for CR[61,68,70,71]. The more recent theoretical models are based on the chemical equilibrium between free hydronium ions and acid functional groups regularly arranged on a 2D substrate, following the reaction $\mathrm{HA} \rightleftharpoons \mathrm{H}^+ + \mathrm{A}^-$, corresponding to protonation/deprotonation of surface sites. The equilibrium number of deprotonated sites determines the surface charge, which depends on the electrostatic potential, solution pH[61,68], and intrinsic pK_a of surface groups. The titration curves can be obtained by varying the amount of acid/base added to the system.

The theoretical descriptions based on the mean-field PB theory are limited in scope to systems in the, so-called, weak coupling limit[1] (*e. g.*, weak electrostatic correlations), and are also unable to address the general case of polyelectrolytes or polyampholytes for which the conformation of a molecule is strongly coupled to the state of protonation of its acid/base groups[72–74]. For such complicated systems, we are forced to rely on computer simulations, which must account for the protonation/deprotonation reactions of polymer's monomers[75–77].

Differently from simulations of simple fluids, implementation of computer simulations for Coulomb systems requires use of advanced techniques to circumvent the problems associated with the long-range nature of the Coulomb force[78–82], which prevents application of the minimal-image periodic boundary condition. Instead, an infinite number of replicas of the system must be considered, alongside with the long-range Coulomb interaction between the ions in these replicas. Ewald summation method can then be used to efficiently perform the sum over the replicas. Nevertheless, a large computational cost is required to simulate dense charged systems, when compared to short-range interacting systems[83,84]. The overall energy of the replicated system depends on the choice of the boundary condition for the resulting crystal of the periodic replicas (tin-foil, vacuum, slab), and care must be taken to choose the boundary condition appropriate to the physical situation at hand. Moreover, it is sometimes convenient (if not necessary) to study systems that lack charge neutrality, in which case a proper regularization of the Coulomb interaction must be perform to avoid infinite energies[79]. The presence of acid/base groups poses additional challenges[47,85–87]. When performing MC simulations, the possibility of a reaction between a proton and an adsorption site must be taken into account, in addition to the standard MC moves. This defines a reactive Monte Carlo (rMC) simulation, in which equilibrium is established considering MC moves that account for the protonation/deprotonation reactions, in a way that satisfies the detailed balance condition[47,88–90]. Furthermore, in a canonical simulation, "potential of hydrogen" defined as $\mathrm{pH} = -\log_{10}(a_H)$ — where the proton activity is $a_H = \frac{c_H}{c^\ominus} \mathrm{e}^{-\beta\mu_{ex}}$, c_H is the average concentration of free hydroniums inside the simulation at equilibrium, $c^\ominus = 1$ M is the standard concentration, μ_{ex} is the excess electrochemical potential of a hydronium ion, and $\beta = 1/k_B T$ is the inverse thermal energy — is not known *a priori* and must be calculated separately after the equilibrium has been achieved. In principle, a_H can be obtained *via* the traditional Widom insertion method[91]. In practice, however, the calculation becomes inaccurate due to the typically small number of hydronium ions inside the simulation cell for intermediate and large pH values. Moreover, insertion of a hydronium ion results in a charge non-neutral periodic system, requiring special techniques to avoid divergence of the excess chemical potential. A recently proposed alternative simulation method, designed to circumvent these difficulties, relies on the surface Widom insertion algorithm with a special technique for computing the change in the Coulomb energy when a virtual proton is inserted into the system[77,91,92].

The goal of the present work is to use the canonical rMC simulations to explore the role of electrostatic correlations in CR in suspensions containing multivalent ions. We will demonstrate that a modified mean-field theory is able to correctly account for the CR in suspensions containing multivalent *coions* – showing that electrostatic correlations are only marginally important in such systems. On the other hand, for systems with multivalent *counterions*, the mean-field theory fails dramatically, demonstrating that electrostatic correlations are of fundamental importance for CR in suspensions with multivalent counterions.

The outline of this work is as follows. In Section II, the setup of the system under consideration is briefly described. The canonical rMC simulations with multivalent anions are reviewed in Section III. Next, the theoretical approach of canonical CR is discussed in Section IV. Results are shown and discussed in Section V, followed by the closing remarks and perspective of new developments in Section VI. Finally, the detailed calculations of the electrostatic correlations contributions to the free energy, which are included in the modified PB equation, are provided in the Appendix A.

II. SYSTEM

In this work, we will consider two different cell models: a spherical hard cell of radius R_c with hard boundary (SHC), and a cubic cell of volume L^3 with periodic boundary conditions in all three directions (PC).

We consider a spherical nanoparticle of radius a, placed at the center of the cell. In the case of a SHC, the cell

radius R_c is related to the volume fraction, η, of the nanoparticles inside the suspension, $\frac{R_c}{a} = \eta^{-1/3}$, as sketched in Fig. 1 a. In the case of a PC, $\eta = 4\pi a^3/3L^3$. At the start of the simulation a nanoparticle contains Z fully ionized acidic groups, each of acid dissociation constant K_a, uniformly distributed over its surface. The cell also contains fully ionized 1:z_- electrolyte of concentration c_s, resulting in a total of N_s anions of valence z_- and $N_+ = z_- N_s$ monovalent cations. In addition, Z of hydronium ions are added to preserve the overall charge neutrality. All ions are free to move within the cell volume. For simplicity, we assume that all ions are equal-sized, of radius $r_i = 2$ Å. Water is treated implicitly as a uniform dielectric medium of Bjerrum length $\lambda_B = q^2/k_B T\epsilon = 7.2$ Å. The equilibrium charge of the nanoparticle is $-Z_{eff}q$, where Z_{eff} is the average number of deprotonated surface groups after the surface reaction $\mathrm{H^+ + A^-} \rightleftharpoons \mathrm{HA}$ reaches equilibrium. Note that *a priori* we do not know either the concentration or activity of free protons inside the system. These can only be calculated after the simulation is fully equilibrated. To change the pH inside the system we can add a base, such as NaOH. Since the dissociation of water is so weak, addition of a base molecule will result in the reaction between a hydronium ion and a base molecule, resulting in formation of a water molecule and release of Na^+. In the present implicit water model, the net effect will be the replacement of a hydronium ion by a sodium ion, $H_3O^+ \rightarrow Na^+$. We can then rerun the simulation with $Z-1$ hydroniums and one extra Na^+ to obtain the new charge of the nanoparticle. The new equilibrium pH can then be calculated using the algorithm described later on in this paper[93]. Repeating this procedure – *i.e.* adding more base molecules – we can explore the full pH range, obtaining the complete titration curve for a suspension of nanoparticles.

For the SHC, the electrostatic energy is given by the usual Coulomb law:

$$E = \sum_{i=1}^{N-1} \sum_{j=i+1}^{N} \frac{q_i q_j}{\varepsilon |\boldsymbol{r}_i - \boldsymbol{r}_j|}, \tag{1}$$

where the sum is performed over all charged species (both ions and sites), and ε is the water permittivity. On the other hand, for PC the electrostatic energy of the system is obtained using the Ewald summation technique:

$$\begin{aligned} E = & \frac{1}{2} \sum_{ij}{}' \sum_{\boldsymbol{n}} \frac{q_i q_j \mathrm{erfc}(\kappa_e |\boldsymbol{r}_i - \boldsymbol{r}_j - L\boldsymbol{n}|)}{\varepsilon |\boldsymbol{r}_i - \boldsymbol{r}_j - L\boldsymbol{n}|} \\ & + \sum_{k \neq 0} \frac{2\pi \exp(-\boldsymbol{k}^2/4\kappa_e)}{\varepsilon V \boldsymbol{k}^2} (A(\boldsymbol{k})^2 + B(\boldsymbol{k})^2) \\ & - \sum_i \frac{q_i^2 \kappa_e}{\varepsilon \sqrt{\pi}} - \frac{Q_t^2}{2\varepsilon V \kappa_e^2}, \end{aligned} \tag{2}$$

where

$$\begin{aligned} A(\boldsymbol{k}) &= \sum_i q_i \cos(\boldsymbol{k} \cdot \boldsymbol{r}_i), \\ B(\boldsymbol{k}) &= \sum_i q_i \sin(\boldsymbol{k} \cdot \boldsymbol{r}_i), \end{aligned} \tag{3}$$

$\boldsymbol{n} = (n_1, n_2, n_3)$ are integers, and $\boldsymbol{k} = (\frac{2\pi}{L} n_1, \frac{2\pi}{L} n_2, \frac{2\pi}{L} n_3)$ are the reciprocal lattice vectors for the cubic simulation box of side length L and volume $V = L^3$, and κ_e is an arbitrary damping parameter. The expression (2) is also valid for systems with an excess charge $Q_t = \sum_i q_i$ and the corresponding uniform neutralizing background[77,93]. The prime on the sum indicates that the term $i = j$ is excluded from the summation for $\boldsymbol{n} = 0$. We set $\kappa_e = 5/L$, so that only $\boldsymbol{n} = 0$ needs to be considered for the short range – sum over erfc terms – contribution to the electrostatic energy.

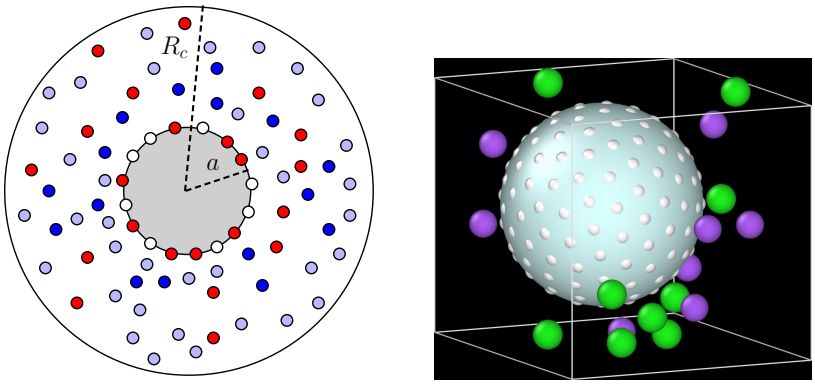

(a) (b)

FIG. 1: a) A two dimensional representation of the system under investigation. A spherical nanoparticle of radius a is placed at the center of a spherical cell of radius R_c (SHC). The particle surface contains Z acid groups regularly arranged over its surface. Each site can be in either protonated (white circles) or deprotonated (red circles) state. The cell also contains hydronium ions (dark blue circles), as well as multivalent anions (red circles) and monovalent Na^+ ions (light blue circles) from dissolved salt of concentration c_s and from the added base. b) 3D representation of the same system inside a periodically replicated cubic cell (PC).

For a cell model with only one colloidal particle located at its center, we expect that the specific boundary condition – hard wall or periodic – should not make a significant difference for thermodynamics. In Fig. 2, we show a comparison of the density profiles of positive and negative ions inside a SHC and PC containing 100 mM of 1:1 or 1:3 electrolyte, for a nanoparticle of $Z = 600$ non-reacting surface groups, obtained using a standard canonical MC. As can be seen, the density profiles for both cases are almost identical. This is very convenient, allowing us to use SHC to construct the mean-field theory of CR. The spherical symmetry of the SHC, makes solution of the nonlinear PB equation much simpler, since it can be transformed into a one dimensional integral equation. On the other hand, PC would require us to solve the full three dimensional non-linear differential equation, which is significantly more involved.

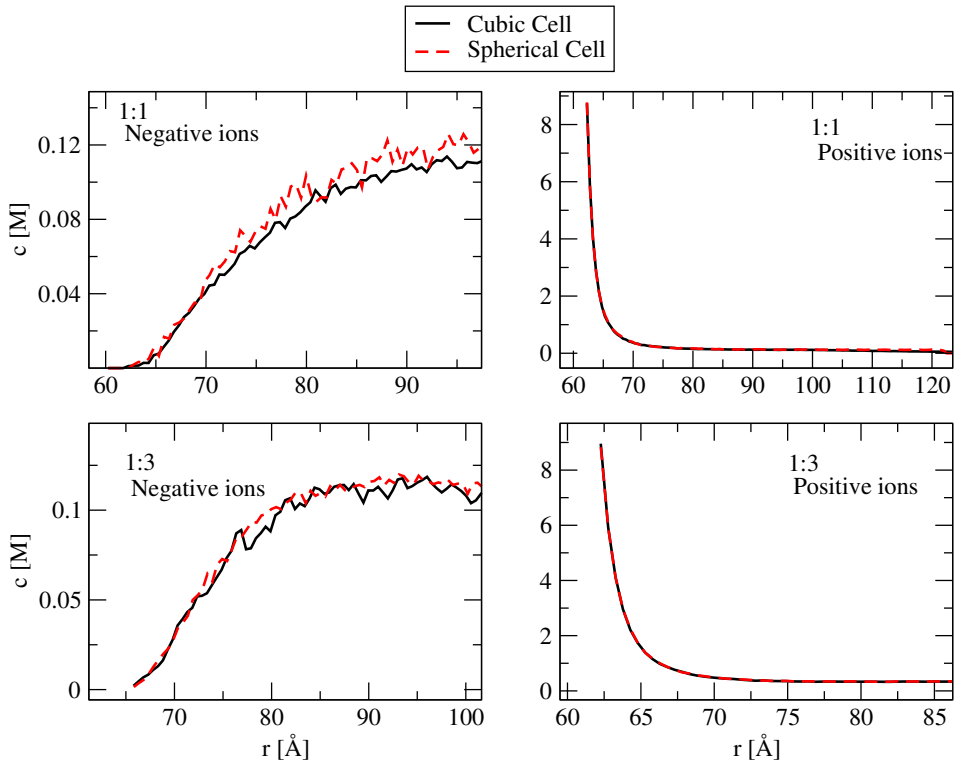

FIG. 2: Comparison of ionic density profiles for a nanoparticle of fixed charge $-600q$. In all cases the concentration of electrolyte is 100mM. The cation density profiles are practically indistinguishable between SHC and PC.

III. REACTIVE CANONICAL MONTE CARLO SIMULATIONS

In a canonical simulation, one does not have a direct access to the chemical potential of hydronium ions necessary to determine pH of the system. This makes canonical titration simulations complicated[90], since pH must be determined separately after equilibrium has been established. Furthermore, a very small number of free hydronium ions present inside the cell makes the usual methods to obtain chemical potential, necessary to calculate pH, very inaccurate. To remedy these problems, we use the recently developed method for canonical titration simulations introduced in the Ref. [93]. Although in the present paper we only consider a PC model with one colloidal particle, the simulation method is completely general and can be applied to a system with an arbitrary number of nanoparticles inside the simulation cell with periodic boundary condition.

For a canonical reactive MC, the simulation approach involves two distinct types of moves: bulk moves, for which ion positions undergo random change with the acceptance probabilities determined by the standard Metropolis algorithm, and reaction protonation/deprotonation, $\mathrm{HA} \rightleftharpoons \mathrm{H}^+ + \mathrm{A}^-$, moves. When a proton moves from the bulk and reacts with an active site on the surface, both electrostatic and chemical energies of the system change. The chemical energy associated with transferring a proton from the bulk to the surface is $k_BT \ln \frac{\mathrm{K}_a}{c^\ominus}$, where K_a is the surface acid dissociation constant. The change in electrostatic energy of the system can be calculated using Eq. (2). The acceptance probability for a protonation move is then given by[90,93]:

$$\mathrm{P}_p = \min\left[1, \frac{N_\mathrm{H}}{V N_A \mathrm{K}_a} e^{-\beta \Delta E}\right], \tag{4}$$

while for a deprotonation it is:

$$\mathrm{P}_d = \min\left[1, \frac{V N_A \mathrm{K}_a}{N_\mathrm{H} + 1} e^{-\beta \Delta E}\right], \tag{5}$$

where N_A is the Avogadro number, N_H is the number of free hydronium ions, and ΔE is the change in electrostatic energy after the protonation/deprotonation move, calculated using Eq. (2). Once the system is fully equilibrated and the average number of protonated surface groups N_p is obtained, we can use the surface Widom insertion algorithm

to calculate the pH of the suspension[93]:

$$\mathrm{pH} = -\log_{10}\left(\frac{N_p+1}{Z}\right) + \mathrm{pK}_a + \log_{10}\left(\left\langle \mathrm{e}^{-\beta(\Delta E + q\phi_B)}\right\rangle_0\right), \tag{6}$$

where ϕ_B is the Bethe potential of the periodically replicated system, $\phi_B = -\frac{2\pi}{3\varepsilon_w V}\sum_i q_i {\boldsymbol{r}_i}^2$. The surface Widom method involves introduction of a virtual proton into the system, which then reacts with one of the surface sites. If the randomly chosen site is already protonated, this results in $\Delta E = \infty$, otherwise the energy of the virtual protonate state is calculated neutralizing the charge of the selected site, $-q \to 0$. Since the virtual proton is periodically replicated when it is introduced into the system, we must also include the corresponding neutralizing background. The resulting change in the electrostatic energy, ΔE, can be calculated using Eq. (2). The intrinsic pK_a of the reaction is defined as $\mathrm{pK}_a = -\log_{10}(\mathrm{K}_a/c^{\ominus})$, where $c^{\ominus} = 1$ M is the standard concentration. The subscript 0 on the brackets in Eqn. (6) indicates that the evolution of the system in between the virtual proton insertions is performed using the Hamiltonian of the unperturbed (without virtual proton) system.

IV. CANONICAL FORMULATION OF THE CHARGE REGULATION THEORY

To construct a canonical theory of CR, we consider a nanoparticle of Z acidic surface sites inside a SHC of free volume $V_0 = \frac{4\pi}{3}(R_c^3 - a^3)$. In equilibrium, Z_{eff} of surface sites will remain deprotonated. The bulk of the cell contains N_H free hydronium ions and $Z_{eff} - N_H$ monovalent Na^+ ions. The cell also contains a 1:z_- electrolyte of concentration c_s . The total number of monovalent cations (counterions) is $N_+ = z_- c_s V_0 + Z_{eff}$ and the number of z_--valent anions (coions) is $N_- = c_s V_0$. All ions are modeled as hard sphere of radius r_i, with a point charge located at their center. The cations, anions, and hydronium ions are free to move through out the free volume V_0. There is a chemical equilibrium between the free hydroniums and the protons adsorbed to the nanoparticle's surface. The goal of the theory is to calculate Z_{eff}, for a given number of free hydroniums N_H and electrolyte of concentration c_s, and then relate these to the pH inside the SHC.

Working in the framework of canonical ensemble, the equilibrium distributions of ionic species, subject to the nanoparticle's electric field, follow from the stationary condition[1,94]

$$\frac{\delta \mathcal{F}}{\delta \rho_i(\boldsymbol{r})} = \mu_i, \tag{7}$$

where $\mathcal{F}$ represents the Helmholtz free energy and μ_i are the Lagrange multipliers that ensure the fixed number of particles of type i inside the cell. This relation can be interpreted as expressing the condition of constant electrochemical potential of each specie i inside the system.

The Helmholtz free-energy functional $\mathcal{F}$ is composed of the entropic (ideal gas) contribution $\mathcal{F}^{id}$, a mean-field contribution $\mathcal{F}^{mf}$, and a (generally unknown) excess[95] free-energy $\mathcal{F}^{ex}$. The ideal contribution is explicitly given by

$$\mathcal{F}^{id} = \sum_i \int \rho_i(\boldsymbol{r})[\ln(\Lambda_i^3 \rho_i(\boldsymbol{r})) - 1]d\boldsymbol{r}, \tag{8}$$

where Λ_i denotes the thermal wavelength of a specie i. The mean-field contribution reads

$$\mathcal{F}^{mf} = \sum_i \int \frac{q z_i \rho_i(\boldsymbol{r'})\varrho(\boldsymbol{r})}{\varepsilon|\boldsymbol{r}-\boldsymbol{r'}|} d\boldsymbol{r}d\boldsymbol{r'} + \frac{q^2}{2}\sum_{i,j}\int \frac{z_i z_j \rho_i(\boldsymbol{r})\rho_j(\boldsymbol{r'})}{\varepsilon|\boldsymbol{r}-\boldsymbol{r'}|} d\boldsymbol{r}d\boldsymbol{r'}, \tag{9}$$

where q is the proton charge. The sum is performed over the ionic species of valence z_i, and $\varrho(\boldsymbol{r}) = -\dfrac{Z_{eff}q}{4\pi a^2}\delta(r-a)$ is the uniform charge density at the nanoparticle surface arising from the deprotoneted sites. Application of the Euler-Lagrange condition (7) leads to the general relation

$$\ln\left[\Lambda_i^3 \rho_i(\boldsymbol{r})\right] + \beta q z_i \varphi(\boldsymbol{r}) + \beta \mu_i^{ex}(\boldsymbol{r}) = \beta\mu_i \equiv \ln\left(\Lambda_i^3 \bar{c}_i\right), \tag{10}$$

where $\varphi(\boldsymbol{r})$ is the mean electrostatic potential,

$$\varphi(\boldsymbol{r}) = \sum_i \int \frac{q z_i \rho_i(\boldsymbol{r'})}{\varepsilon|\boldsymbol{r}-\boldsymbol{r'}|} d\boldsymbol{r'} + \int \frac{\varrho(\boldsymbol{r'})}{\varepsilon|\boldsymbol{r}-\boldsymbol{r'}|} d\boldsymbol{r'}, \tag{11}$$

and the position-dependent excess chemical potential is defined as $\mu_i^{ex}(r) = \dfrac{\delta \mathcal{F}^{ex}}{\delta \rho_i(r)}$. We note that, due to the rotational symmetry with respect to both azimuthal and polar angles, the ionic distributions are functions of the radial coordinate r alone, and the above integrals simplify to

$$\varphi(r) = -\frac{Z_{eff} q}{\varepsilon r} + \frac{4\pi q}{\varepsilon r} \sum_i \left[\int_a^r z_i \rho_i(r') r'^2 dr' + r \int_r^{R_c} r' \rho_i(r') dr' \right]. \tag{12}$$

The first term of the rhs of this equation is the isotropic potential due to the nanoparticle, whereas the other contributions represent the potential due to the ionic species. The same result can be easily obtained by a direct application of the Gauss Law and the underlying radial symmetry. The electrostatic potential is set to zero at the cell boundary $r = R_c$, where the electric field also vanishes due to the overall charge neutrality inside the SHC.

The lhs of Eq. (10) can be interpreted as the electrochemical potential of ionic specie i at position r. The equilibrium condition then establishes that this electrochemical potential must be constant everywhere. Relation (10) leads to the following equilibrium concentrations:

$$\rho_i(r) = \bar{c}_i \exp\left[-\beta q z_i \varphi(r) - \beta \mu_i^{ex}(r)\right]. \tag{13}$$

In the present canonical formalism, the coefficients $\bar{c}_i$ must be determined from the constraint of fixed number of ions of each type, N_i, inside the SHC. Using Eq. (13), these coefficients can be evaluated as

$$\bar{c}_i = \frac{N_i}{4\pi \displaystyle\int_a^{R_c} r^2 e^{-\beta q z_i \varphi(r) - \mu_i^{ex}(r)} dr}, \tag{14}$$

and can, therefore, be interpreted as the functionals of ionic density profiles.

The coefficients $\bar{c}_i$ in Eq. (10) are defined as $\bar{c}_i \equiv \dfrac{e^{\beta \mu_i}}{\Lambda_i^3}$. Furthermore, we can split the total electrochemical potential μ_i into the ideal gas and the excess contribution, $\beta \mu_i = \ln(\Lambda_i^3 c_i) + \beta \mu_i^{ex}$, where the mean ionic concentration is $c_i = N_i / V_0$. Note that μ_i^{ex} contains all the interactions, including the contribution from the mean field electrostatic potential. The activity a_H of hydronium ions is then:

$$a_H = \frac{c_H e^{-\beta \mu_H^{ex}}}{c^{\ominus}} = \frac{\bar{c}_H}{c^{\ominus}}, \tag{15}$$

and can be calculated directly using Eq. (14), if the electrostatic potential and the local excess chemical potential $\mu_H^{ex}(r)$ inside the cell are known.

The local excess chemical potentials $\mu_i^{ex}(r)$ in Eq. (10) accounts for the ionic finite size effects and the electrostatic correlations[96,97]. Since in this paper we will only consider solutions of low salt concentrations, under 1M, the steric effects can be ignored – except for the formation of the Stern layer at the surface of a nonoparticle. The electrostatic correlations between ions result in ionic repulsion from a neutral hard wall. This can be understood as follows[96]. In the bulk of suspension, ion electric field is screened by the counterion cloud, resulting in a negative electrostatic solvation free energy. Presence of a wall breaks the spherical symmetry of the ionic cloud, diminishing the screening of electric field produced by the ion and, therefore, the magnitude of the (negative) electrostatic solvation free energy. This results in an effective repulsion of ions from a neutral hard wall. For monovalent ions this effect is small and can be neglected, on the other hand for multi-valent ions it becomes significant. The solvation free-energy can be readily computed using Green function formalism (for details, see Appendix A). Neglecting the curvature effects we obtain:

$$\beta \mu_i^{ex}(r) \equiv \beta W_i(r) = \frac{z_i^2 \lambda_B}{2} \mathcal{W}_0 \left(e^{-2\kappa(r - a - r_i)} + e^{2\kappa(r + r_i - R_c)} \right), \tag{16}$$

where

$$\mathcal{W}_0 = \int_0^{\infty} \left(\frac{p - k}{p + k} \right) \frac{k}{p} dk, \tag{17}$$

and $\kappa = \sqrt{4\pi \lambda_B \sum_i c_i z_i^2}$ is the characteristic inverse Debye screening length inside the cell and $p \equiv \sqrt{k^2 + \kappa^2}$.

For a given Z_{eff} and $\{N_i\}$, the modified PB (mPB) equation, described by the set of equations (12), (13), (14) and (16) can be solved numerically to determine the ionic distributions and the mean electrostatic potential by means of Picard iteration algorithm. First, guess functions are assigned for the density profiles $\rho_i(r)$. Using Eq. (11), the

corresponding electrostatic potential can be calculated. Then, Eqs. (14), (16) and (13) can be used to estimate a new set of density profiles. The procedure is repeated until convergence is achieved. This process allows one to calculate the equilibrium distributions for a given number of hydronium ions N_H and Z_{eff}. However, the solution obtained thus far is not self-consistent, in the sense that the charge regulation effect was not taken into account. Indeed, the number of deprotonated groups, Z_{eff}, is controlled by the chemical equilibrium between free hydroniums and the adsorbed protons. Following Ref. [98], we can determine Z_{eff} using a two state model:

$$Z_{eff} = Z\frac{e^{-\beta f_0}}{e^{-\beta f_0}+e^{-\beta f_1}} = \frac{Z}{1+e^{-\beta\Delta\mu}}, \tag{18}$$

where f_0 is the free energy of the system when a site is deprotonated, f_1 is when it is protonated, and $\Delta\mu = f_1 - f_0$ is the free energy change of the system due to the removal of proton from the bulk of the cell and its reaction with the adsorption site. In the initial state the site is deprotonated and is solvated by the ions of electrolyte solution, resulting in solvation free energy (see Appendix A):

$$\beta\mu_{sol} = \frac{\lambda_B}{2}\int_0^\infty \left(\frac{k-p}{p+k}\right) e^{-2kr_i} dk, \tag{19}$$

where r_i is the hydrated ionic radius, *i.e.* the distance of the closest approach of ions to the surface. The proton in the bulk has free energy μ_H. After the protonation, there is a chemical free energy gain associated with the formation of a covalent bond between the proton and the site. This energy can be expressed in terms of the acid dissociation constant K_a as $k_BT\ln\left(\mathrm{K}_a\Lambda_H^3\right)$. Furthermore when proton becomes bound to the site, it still interacts electrostatically with all the other deprotonated sites as well as with all the other ions inside the solution, resulting in an electrostatic energy $q\phi$. Therefore,

$$\beta\Delta\mu = \ln\left(\mathrm{K}_a\Lambda_H^3\right) + \beta q\phi - \beta\mu_{sol} - \beta\mu_H. \tag{20}$$

Substituting this into Eq. (18), we can rewrite it as

$$Z_{eff} = \frac{Z}{1+10^{(pK_a-pH)}e^{-\beta q\phi+\beta\mu_{sol}}}. \tag{21}$$

This expression might give a misleading impression that the effective charge is determined solely by the difference $\mathrm{pH}-\mathrm{pK}_a$ alone. This, however, is not the case[90], since the electrostatic contribution depends on the pH non-trivially in virtue of the relation (14).

In order to calculate the electrostatic contribution ϕ, discreteness of sites must be taken into account[98]. Following, Ref [98], we can split ϕ into the mean-field and discrete surface charge contributions $\beta q\phi = \beta q\varphi(a) + \beta q\varphi_{disc}$. The mean-field $\varphi(a)$ is determined by the solution of the PB equation, while the effects due to the discreteness of the surface sites are included using the theory of one component plasma (OCP) resulting in[98]

$$\beta\varphi_{disc} = \frac{\lambda_B M Z_{eff}}{a\sqrt{Z}}, \tag{22}$$

where $M \approx 1.106$ is the Medulung constant of the two dimensional triangular lattice.

Equation (21) can now be solved self-consistently in a combination with the mPB equation. We proceed as follows. For a given value of pK_a and ions of each type inside the cell $\{N_i\}$, we "guess" the mean-electrostatic potential inside the suspension $\varphi_{guess}(r)$. For this guess we calculate the ionic density profiles using Eq. (13) and pH using Eq. (15). We then solve Eq. (21) to obtain Z_{eff}. Using this value and the ionic density profiles we then recalculate the electrostatic potential using Eq. (12), and repeat this procedure until convergence is achieved. The full titration curve can be obtained by varying the number of free hydronium ions inside the cell N_H for a fixed concentration of salt ions.

V. RESULTS

We shall now employ both simulations and theory to investigate CR mechanism in suspensions containing multivalent ions. The results presented are for weak acidic surface groups of $\mathrm{pK}_a = 5.4$. All ions are treated as hard spheres of radius $r_i = 2$ Å. Nanoparticles are hard spheres of radius $a = 6$ nm with Z surface adsorption sites. For theory we will use SHC of radius $R_c = 12.4$ nm. To explore the accuracy of the mPB equation, we start by considering nanoparticles of fixed charge. Once convinced of the accuracy of the mPB approximation for 1:z electrolyte, we will proceed to investigate charge regulation and construct the tritation isotherms, which we will then compare to simulations for different salt concentrations and charge asymmetries.

A. Ionic profiles

To test the accuracy of the mPB equation for suspensions with multivalent coions, we calculate the ionic density profiles for nanoparticles of fixed charge $-Zq$. Fig. 3 shows ionic profiles around a nanoparticle of charge $Z = 200$, in a suspensions containing 1:3 electrolyte of various concentrations: $c_s = 20$ mM (a), $c_s = 100$ mM (b) and $c_s = 150$ mM (c). A very good agreement is observed in all cases. The reason for such good agreement is due to the absence of strong electrostatic correlations between ions in the vicinity of the charged surface – because of their strong repulsion from the charged surface the concentration of multivalent coion remains low everywhere. We also note that, since ionic radius is small and the concentrations are not too large, the packing effects close to the surface are insignificant. As the result, steric interactions among the condensed counterions – which are completely neglected at the mean-field level – are negligible. Furthermore, since the counterions are monovalent, electrostatic correlations between them remain weak near the charged surface. The trivalent coions, on the other hand, are strongly repelled from the surface. Since the surface charge is not very large, the counterion concentration close to the surface is not sufficient to produce a neighboring layer of trivalent coions (the so-called layering effect), again signifying that ionic correlations are small in this range of ionic concentration and surface charge, and are well described by Eq. (16).

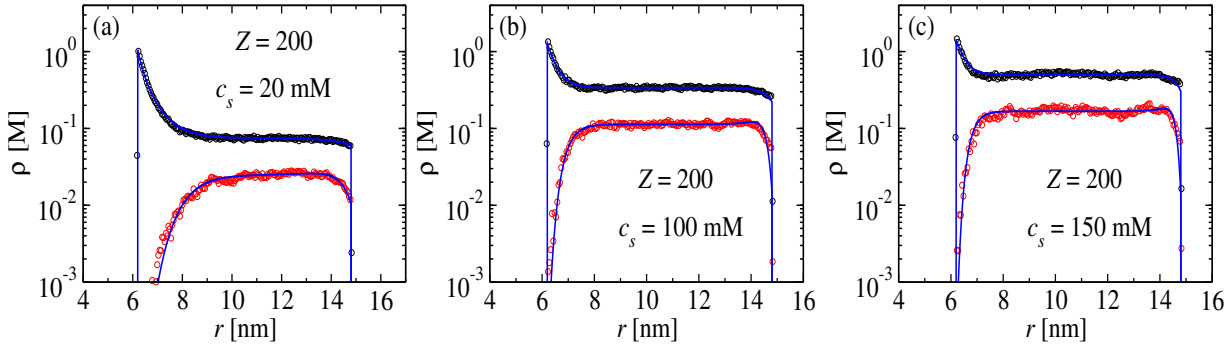

FIG. 3: Ionic profiles around a nanoparticle of radius $a = 6$ nm, and a fixed charge of $-200q$. Black and red symbols are simulation results for monovalent cations and trivalent anions, respectively, while blue curves are the corresponding theoretical predictions. The mean salt concentrations are $c_s = 20$ mM (a), $c_s = 100$ mM (b) and $c_s = 150$ mM (c).

Similar trends can be observed in Fig. 4, which shows the density profiles for the same set of salt concentrations, but in a regime of much higher surface charge, $Z = 1200$. Despite the buildup of a much larger and thinner layer of counterions at the surface, the ionic correlations are not large enough to result in any significant deviation from the mean-field predictions. This again is a consequence of weak electrostatic correlations among monovalent counterions at the surface[1]. If counterions were trivalent and coions monovalent, the repulsion between neighboring counterions close to the surface would result in strong deviations from the mean-field predictions[99]. It is thus important to emphasize that the validity of the mPB equation is restricted to the case of monovalent counterions and the surface charge and salt concentrations that are not too large. In the case of trivalent counterions, strong electrostatic correlations will restrict considerably the range of validity of the mean-field approach[1].

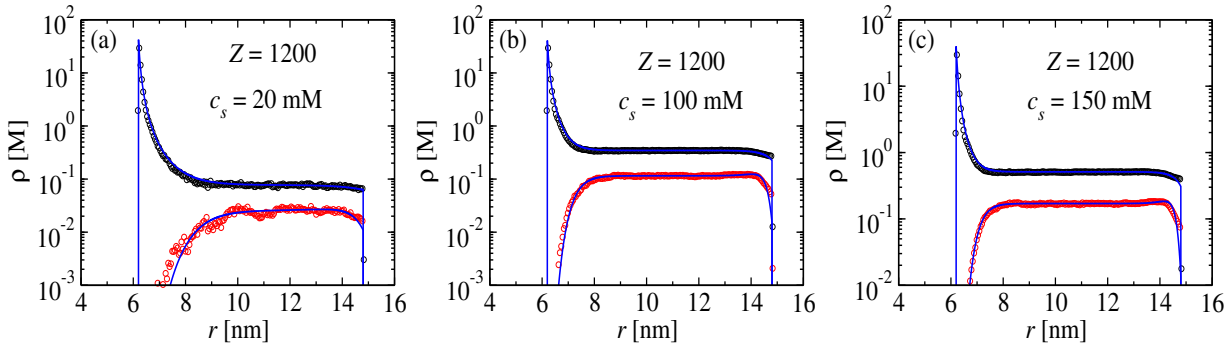

FIG. 4: Ionic profiles around a nanoparticle of radius $a = 6$ nm, and a fixed charge of $-1200q$. Black and red symbols are simulation results for monovalent cations and trivalent anions, respectively, while blue curves are the corresponding theoretical predictions. The mean salt concentrations are $c_s = 20$ mM (a), $c_s = 100$ mM (b) and $c_s = 150$ mM (c).

Perhaps the most interesting feature of the comparisons presented in Figs. 3 and 4 is the ability of the mPB equation to accurately describe the ionic depletion close to the cell boundary. This depletion is clearly more pronounced for multivalent coions and is a consequence of electrostatic correlations. The correlations between ions result in counterion clouds that screen ionic electric field inside the electrolyte. The distortion of the polarization cloud produced by the wall prevents efficient screening, resulting in a repulsion from the wall. This effect is stronger for trivalent ions, which feel greater repulsion from a neutral hard wall. In order to emphasize this point, in Fig. 5 a comparison is shown between the distributions of monovalent and trivalent anions around a nanoparticle of charge $Z = 600$. In the case of $1:3$ electrolyte, a larger depletion zone is observed around the nanoparticle, which is mainly of electrostatic nature. At the same time, a strong repulsion of trivalent anions from the neutral cell boundary can be seen.

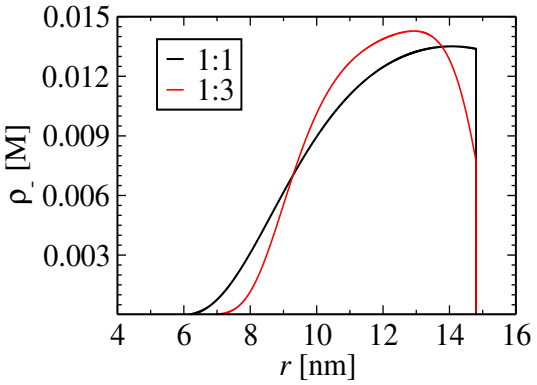

FIG. 5: Comparison between coion distributions calculated using the mPB equation, for the case of 1:1 (black curve) and for the case of $1:3$ (red curve) electrolytes. In both cases $c_s = 10$ mM. The nanoparticle charge is fixed at $-600q$ and radius $a = 6$ nm.

The mPB equation, therefore, captures the most important electrostatic correlation effects present in $1{:}z$ electrolytes. This is not the case for the usual PB equation without the electrostatic solvation correction, in which case the profiles near a hard wall remain the same as in the bulk. We should stress that a proper description of such depletion effect is quite important, since the contact theorem[100–105] allows us to connect the ionic density at the hard wall with the osmotic pressure that exists inside the suspension.

B. Tritation curves

Having established the accuracy of the mPB equation for ionic density profiles, we proceed to include CR to investigate how variation of pH influences the nanoparticle charge and the osmotic pressure inside the suspension. All the results presented in this section have been obtained for nanoparticles with $Z = 600$ weak acidic sites and size $a = 6$ nm. For very high pH the acidic groups become completely deprotonated resulting in nanoparticles with surface charge density of $\sigma \approx 212.2$ mC/nm^2.

In Fig. 6 we present the titration curves for suspensions of nanoparticles containing 1:2 electrolytes at concentrations: $c_s = 10$ mM (a); $c_s = 50$ mM (b); and $c_s = 100$ mM (c). A perfect agreement between theory and simulations is found for all salt concentrations, in the whole range of pH values. The success of the theory is clearly due to the high accuracy of the mPB equation for predicting the ionic density profiles and due to very accurate description of the electrostatic potential in the vicinity of each site, calculated using the φ_{disc} and μ_{solv}. We observe that for pH $\gtrsim 8$, the number of protonated sites is very low. On the other hand for pH $\lesssim 2$ almost all sites are protonated. Addition of electrolyte leads to screening of electrostatic interactions, resulting in lower protonation for the same value of pH.

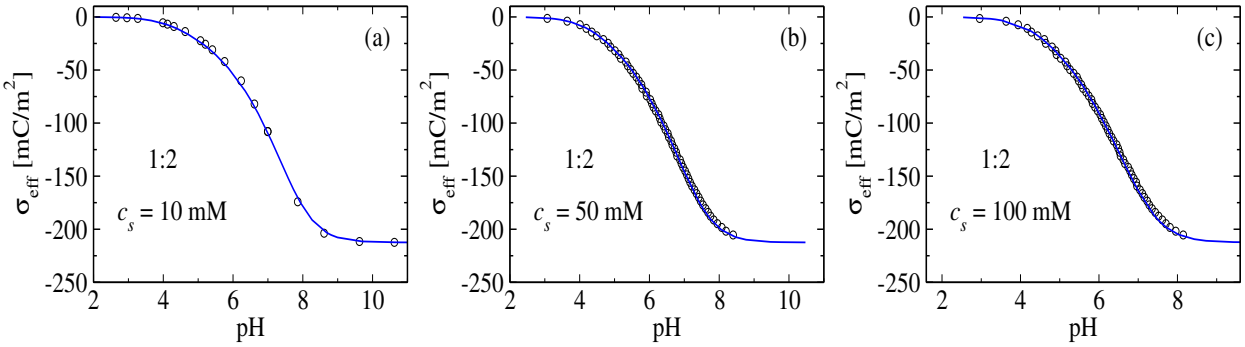

FIG. 6: Tritation isotherms showing the nanoparticle surface charge density as a function of solution pH, in the presence of 1:2 electrolytes of concentrations $c_s = 10$ mM (a), $c_s = 50$ mM (b) and $c_s = 100$ mM (c). Black symbols are the simulation results, whereas the blue solid curves correspond to theoretical predictions.

Titation curves for the case of added 1:3 electrolyte at concentration c_s are shown in Fig. 7. To highlight the effect of larger anionic charge, in the panels we also plot the corresponding titration isotherms of suspensions with 1:1 salt at the same concentration. Again, a very good agreement between simulations and theory is observed for all studied electrolyte concentrations. We see that increase of anion valence results in diminished protonation – larger Z_{eff} – for the same salt concentration and pH. The reason for this is that the large charge of trivalent anions favors their repulsion from the nanoparticle surface, see Fig. 5. This is further amplified by the electrostatic correlations that also favor bulk solvation of trivalent coions. The net result is that compared to 1:1 electrolyte there are fewer trivalent anion present near the surface of a nanoparticle, making the electrostatic potential less negative – and, therefore, attracting less hydronium ions into this region – leading to diminished protonation and larger Z_{eff}.

The difference in protonation between suspensions containing either 1:3 or 1:1 electrolyte is most pronounced at intermediate pH values, in the range pH ~ 5 to pH ~ 7. For example, at pH $= 6.0$ and $c_s = 50$ mM, the the number of deprotonated groups rises from $Z_{eff} \approx 179$ to $Z_{eff} \approx 248$, when z_- is changed from one to three —representing a $\sim 38\%$ increase in the nanoparticle charge.

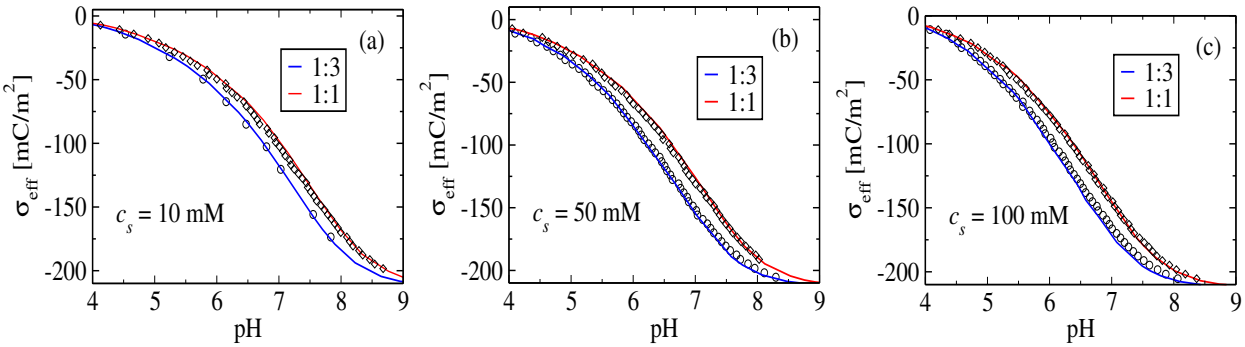

FIG. 7: Tritation isotherms showing the nanoparticle surface charge density as a function of solution pH, in the presence of 1:1 and 1:3 electrolytes of concentrations $c_s = 10$ mM (a), $c_s = 50$ mM (b) and $c_s = 100$ mM (c). Symbols are the simulation results, whereas the blue and red solid curves correspond to theoretical predictions for trivalent and monovalent anions, respectively.

Although the theory proposed in this paper is able to describe very well suspensions containing multivalent coions, we expect it to fail when applied to suspensions containing multivalent counterions, such as Ca^{++}. For such suspensions, both proton and Ca^{++} will compete for the same adsorption sites, leading to strong correlations between the two near the surface of a nanoparticle. Fig 8, compares the tritation curves obtained using the canonical rMC simulations (symbols) with the predictions of the present theory (solid curve) for suspensions containing 2 : 1 electrolyte. As expected, we see strong deviations between the present theory and the simulations. At this time it is not clear how to include the strong electrostatic correlation effects into the theoretical framework presented in this paper.

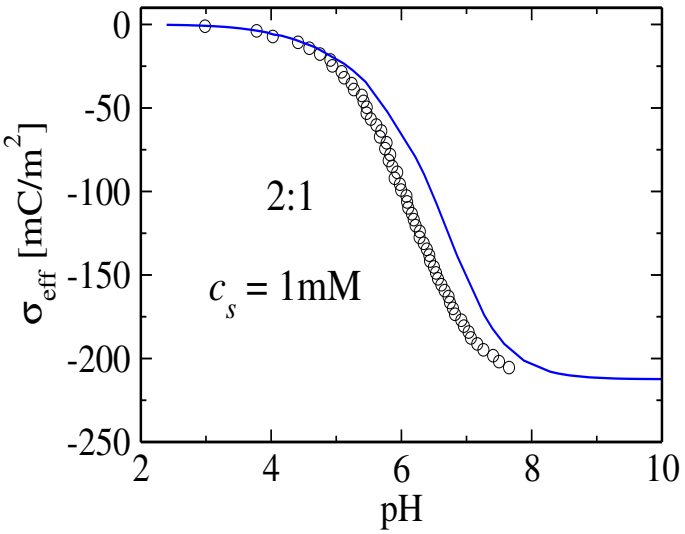

FIG. 8: Comparison of titration isotherms calculated using rMC (symbols) and the present theory (solid blue curve) for suspensions containing $2:1$ electrolyte at concentration $c_s = 1$ mM.

C. Osmotic pressures

One of the advantages of the proposed theoretical framework is its ability to accurately predict the ionic density profiles at the outer boundary of a SHC. This allows us to use the contact-value theorem[100–105] to calculate the osmotic pressure inside the suspension. The exact relation between the osmotic pressure Π and ionic densities at contact with the outer wall of the SHC is

$$\beta\Pi = \sum_i \rho_i(R_c - r_i), \tag{23}$$

where the summation is over all ionic species. This relation establishes that the osmotic pressure, which is constant throughout the system, can be computed *via* the kinetic momentum which is transferred to the hard wall by ion collisions. Accurate calculations of these contact values are not easy, since they usually require access to ionic correlations. Size effects, for example, are known to push particle towards the outer walls, increasing the contact values, whereas electrostatic solvation effects leads to ionic depletion. In the case of small ions at concentrations less than 1 M, the latter effect is the dominant one. In view of the observed accuracy of the propose model to reproduce such depletion effects, it can be used as a promising route to efficiently and accurately compute osmotic pressures as a function of pH and electrolyte concentration inside a suspension.

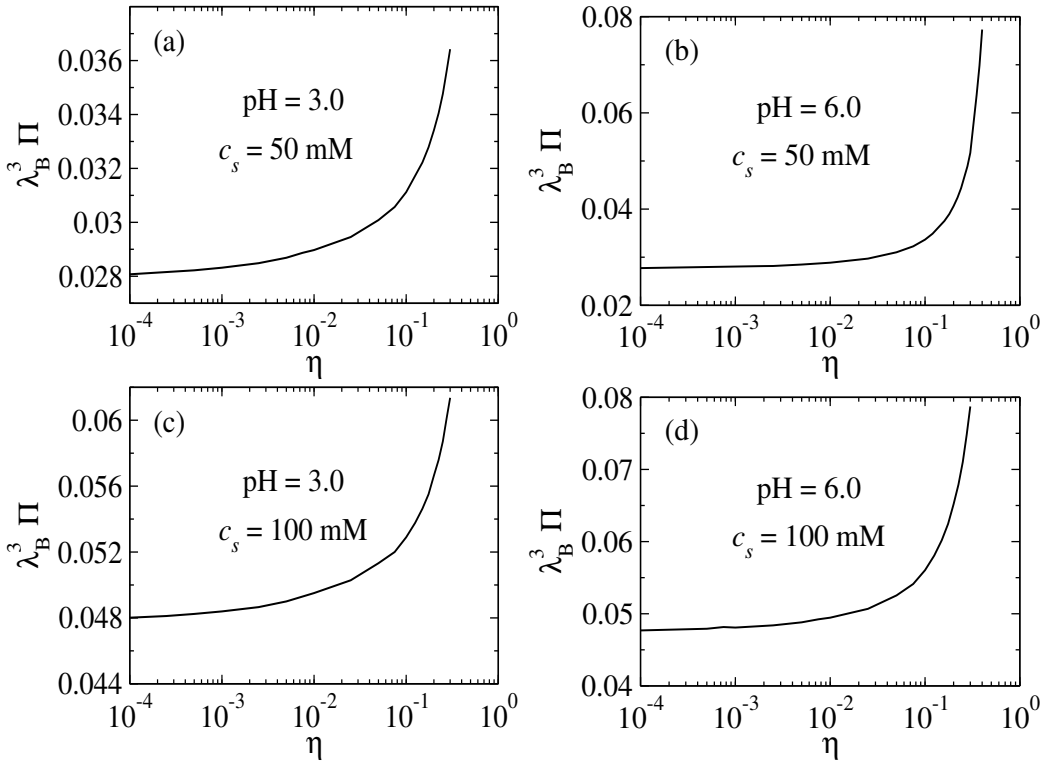

FIG. 9: Osmotic pressures computed from the contact value theorem, Eq. (23), as a function of the packing fraction η, for 1:3 electrolyte at fixed values of solution pH and c_s. In the left panel results are shown for a case where pH = 3, whereas right panels correspond to a higher pH of pH = 6. Two representative salt concentrations are considered: $c_s = 50$ mM (top pannels) and $c_s = 100$ mM (bottom panels).

The osmotic pressures for different pHs and salt concentrations, as a function of the nanoparticle volume fraction η, are shown in Fig 9, for the case of 1:3 electrolytes. At low packing fractions, the osmotic pressures are approximately constant, showing a sharp increase for higher concentrations of the nanoparticles, $\eta \gtrsim 0.1$. For such high volume fractions, the trivalent anions are strongly repelled from the nanoparticle surface and are pushed towards the cell boundary, attracting a large number of monovalent cations into this region as well. This results in a large contact density at the outer SHC surface, leading to a sharp rise in osmotic pressure.

The hydronium concentration is generally much smaller than the concentration of cations from dissolved salt and added base, the main effect of increasing the pH is to increase (in magnitude) the nanoparticle charge. This requires a larger number of base cations inside the cell to preserve the overall charge neutrality. The higher the packing fraction, the larger the concentration of dissolved cations, resulting in higher osmotic pressures. This explains why the pressures increase much stronger at larger η when the pH values are higher (see Fig. 9b) in comparison to the case of smaller pH (see Fig. 9a). This trend is weaker in the case of larger salt concentrations (see bottom panels), when the dominant population of cations arises from the dissociated salt, instead of the added base.

VI. CONCLUSIONS

We have studied CR of nanoparticles in the presence of electrolyte containing multivalent ions. Differently from the earlier approaches which studied CR for a semi-grand canonical system[87,92,98], in which suspension is separated from the reservoir by a semipermeable membrane, the present theory is constructed directly for an isolated suspension (canonical ensemble)[93]. It is important to stress that for a semi-grand canonical system, presence of Donnan potential between system and its implicit reservoir results in titration isotherms (plotted as a function of reservoir pH) that can be very different from those of an isolated system[77,93,106]. Furthermore, we stress that the usual constant pH simulation methods allow us to control only the pH of the reservoir and not the pH of the system[107]. The theory presented in this paper applies directly to isolated suspensions, without invoking an external reservoir. The comparison with simulations shows that the theory is very accurate for suspensions containing 1:z electrolytes at all pH values. The theory is also able to accurately predict ionic depletion close to hard walls — this depletion is driven by the

electrostatic correlations between cations and anions of electrolyte. Taking advantage of the good accuracy of the theory for predicting the ionic density profiles, we have used the well-known contact value theorem to calculate the osmotic pressure of suspensions of nanoparticles for different pH values and salt concentrations. We have also shown that if suspension contains multivalent counterions, the present theory looses its accuracy. This is a consequence of strong electrostatic correlations between the multivalent cations and the adsorbed protons, which cannot be accounted for in the framework of the present theory. This will be the subject of the future work.

VII. ACKNOWLEDGMENTS

This work was supported by CAPES, CNPq, INCT-FCx, and FAPERGS.

Appendix A: Electrostatic correlations contributions

Here we present a detailed calculation of the solvation free energy for ions in the bulk and for surface charge groups. To this end, we calculate the electrostatic potential produced by a point charge q', located a distance z from a hard wall placed inside an electrolyte solution. If the screening length is much smaller than the nanoparticle radius, $\kappa a \gg 1$, the curvature effects can be ignored (as far as the electrostatic solvation energy is concerned), and the nanoparticle interface can be modeled as a flat surface located at $z = 0$. We separate the system into two regions: $-\infty < z < d$, which contains the hard wall, but no electrolyte due to hardcore repulsion of ions from the wall, and $z > d$, where electrolyte is present. The distance d corresponds to the distance of closest approach between the ions and the hard interface. We consider separately the cases in which the test-charge is placed inside the region $0 \leq z \leq d$ (region without electrolyte) and $z > d$ (inside the electrolyte).

1. Test-charge at $z > d$

Using cylindrical coordinate system, the position of the point charge can be represented by (S', θ', z'). Moreover, due to the translational symmetry over the plane, we can set the radial coordinate $S' = 0$, without loss of generality. The azimuthal symmetry, means that the electrostatic potential does not depend on θ. For $z > d$, the electrostatic potential at (S, z) then satisfies the Helmholtz equation with a source term:

$$(\nabla^2 - \kappa^2)G(S, z, z') = -\frac{4\pi q'}{\varepsilon}\delta(z - z')\frac{\delta(S')}{2\pi S'}, \tag{A1}$$

where $\nabla^2 = \frac{1}{S}\frac{\partial}{\partial S}\left(S\frac{\partial}{\partial S}\right) + \frac{\partial^2}{\partial z^2}$. For $z < d$, the potential satisfies the Laplace equation, $\nabla^2 G = 0$. In virtue of the azimuthal symmetry, it is convenient to express the potential in terms of the Bessel function of zeroth order $J_0(kS)$ as:

$$G(S, z, z') = \int_0^\infty g(z, z'; k)J_0(kS)kdk. \tag{A2}$$

The completeness relation for the Bessel functions requires that[108]

$$\frac{\delta(S)}{S} = \int_0^\infty kJ_0(kS)dk. \tag{A3}$$

Substituting Eqs. (A2) and (A3) into Eq. (A1) yields

$$\frac{\partial^2 g}{\partial z^2} - p^2 g = -\frac{2q'}{\varepsilon}\delta(z - z'), \tag{A4}$$

for $z > 0$, where $p^2 = k^2 + \kappa^2$. Here, use was made of the relation $\frac{1}{S}\frac{\partial}{\partial S}\left(S\frac{\partial J_0(kS)}{\partial S}\right) = -k^2 J_0(kS)$. Similarly, using the expression (A2) in Laplace equation, we obtain:

$$\frac{\partial^2 g}{\partial z^2} - k^2 g = 0, \tag{A5}$$

when $z < d$. Equations (A4) and (A5) must be solved subject to conditions of: continuity $g(z, z'; k)$ at $z = d$; discontinuity of derivative at $z = z'$, $g'(z \to z'_-, z; k) - g'(z \to z'_+, z'; k) = \frac{2q'}{\varepsilon}$; and symmetry under the exchange of the source and the observation point $z \longleftrightarrow z'$. In addition, the function $g(z, z'; k)$ must be bounded in the limits $|z| \to \infty$. Solving Eqs. (A4) and (A5) with these constraints, we obtain:

$$g(z, z'; k) = \frac{q'}{\varepsilon p}\left[e^{-p|z-z'|} + \frac{p-k}{p+k}e^{-p(z+z'-2d)}\right], \qquad \text{for} \qquad z > d. \tag{A6}$$

The electrostatic potential produced by a point charge placed at z' at an arbitrary point (z, S) can be obtained upon substituting Eq. (A6) into Eq.(A2). In the region of interest $(z > d)$, the potential is comprised by two contributions:

the usual Debye-Hückel (DH) potential of an ion in the bulk electrolyte – first term of Eq. (A6) – and the polarization contribution produced by the wall – second term of Eq. (A6). The effective ion-wall interaction potential is then[96]:

$$W(z) = \frac{q^2}{2\varepsilon}\int_0^\infty \left(\frac{p-k}{p+k}\right)\frac{k}{p}e^{-2p(z-d)}dk \tag{A7}$$

where the relation $J_0(0) = 1$ has been used. The major contribution to the integral comes from $k \to 0$, in which case $p \to \kappa$. A convenient approximation thus amounts to the replacement $e^{-2p(z-d)} \to e^{-2\kappa(z-d)}$, which renders the integration position-independent:

$$W_i(z) = \frac{z_i^2 q^2}{2\varepsilon}e^{-2\kappa(z-d)}\int_0^\infty \left(\frac{p-k}{p+k}\right)\frac{k}{p}dk. \tag{A8}$$

In the case of SHC model there are two surfaces: the nanoparticle surface and the cell wall. Using the superposition approximation we arrive at Eq. (16).

2. Charge in the region $0 \le z < d$

We now consider the situation of a point charge (corresponding to one of the adsorption sites) located in the region free of electrolyte, $-\infty \le z \le d$. The electrostatic potential then satisfies the equations:

$$\nabla^2 G(z,z',S) = -\frac{4\pi q'}{\varepsilon}\delta(z-z')\frac{\delta(S)}{2\pi S}, \tag{A9}$$

for $-\infty < z < d$, and

$$\left(\nabla^2 - \kappa^2\right)G(z,S) = 0 \tag{A10}$$

in the region $z \ge d$. Proceeding as before, and using expressions (A2) and (A3), the function $g(z,z';k)$ now satisfies:

$$\frac{\partial^2 g}{\partial z^2} = \begin{cases} k^2 g - \dfrac{2q'}{\varepsilon}\delta(z-z') & (-\infty < z < d) \\ p^2 g & (z \ge d). \end{cases} \tag{A11}$$

These equations can be solved to yield

$$g(z,z';k) = \frac{q'}{\varepsilon k}\left[e^{-k|z-z'|} + \left(\frac{k-p}{k+p}\right)e^{k(z+z'-2d)}\right] \qquad \text{for} \qquad -\infty < z < d. \tag{A12}$$

Again, the first term of this expression yields the usual Coulomb potential produced by the charge, while the second term is due to the polarization of ions of electrolyte by the electric field produced by the test charge. The solvation free energy of a point charge located on the hard wall ($S' = 0, z' = 0$) is then:

$$\mu_{solv} = \frac{z_i^2 q^2}{2\varepsilon}\int_0^\infty \left(\frac{k-p}{k+p}\right)e^{-2kd}dk. \tag{A13}$$

[1] Y. Levin, "Electrostatic correlations: from plasma to biology," Reports on Progress in Physics **65**, 1577 (2002).
[2] R. Messina, "Electrostatics in soft matter," Journal of Physics: Condensed Matter **21**, 113102 (2009).
[3] V. Dahirel and J. P. Hansen, "Ion-mediated interactions in suspensions of oppositely charged nanoparticles," The Journal of Chemical Physics **131**, 084902 (2009).
[4] J. N. Israelachvili, in *Intermolecular and Surface Forces (Third Edition)*, edited by J. N. Israelachvili (Academic Press, San Diego, 2011) third edition ed., pp. 53–70.
[5] J. P. Bardhan, "Biomolecular electrostatics—i want your solvation (model)*," Computational Science & Discovery **5**, 013001 (2012).
[6] H. Wennerström, "Electrostatic interactions in concentrated colloidal dispersions," Phys. Chem. Chem. Phys. **19**, 23849–23853 (2017).
[7] B. Honig and A. Nicholls, "Classical electrostatics in biology and chemistry," Science **268**, 1144–1149 (1995).
[8] P. Kovacic, "Bioelectrostatics: Review of widespread importance in biochemistry," Journal of Electrostatics **66**, 124–129 (2008).
[9] G. C. Wong and L. Pollack, "Electrostatics of strongly charged biological polymers: Ion-mediated interactions and self-organization in nucleic acids and proteins," Annual Review of Physical Chemistry **61**, 171–189 (2010).
[10] A. G. Cherstvy, "Electrostatic interactions in biological dna-related systems," Phys. Chem. Chem. Phys. **13**, 9942–9968 (2011).
[11] Y. Yang, E. Raee, Y. Zhou, and T. Liu, "The role of electrostatic interaction in the self-assembly of macroions," in *Supramolecular Assemblies Based on Electrostatic Interactions*, edited by M. A. Aboudzadeh and A. Frontera (Springer International Publishing, 2022) pp. 55–84.

[12]A. Krieger, A. Zika, and F. Gröhn, "Functional nano-objects by electrostatic self-assembly: Structure, switching, and photocatalysis," Frontiers in Chemistry **9** (2022), 10.3389/fchem.2021.779360.
[13]A. Kudlay and M. Olvera de la Cruz, "Precipitation of oppositely charged polyelectrolytes in salt solutions," The Journal of Chemical Physics **120**, 404–412 (2004).
[14]A. Hanisch, A. H. Gröschel, M. Förtsch, M. Drechsler, H. Jinnai, T. M. Ruhland, F. H. Schacher, and A. H. E. Müller, "Counterion-mediated hierarchical self-assembly of an abc miktoarm star terpolymer," ACS Nano **7**, 4030–4041 (2013).
[15]A. M. Tom, R. Rajesh, and S. Vemparala, "Aggregation of flexible polyelectrolytes: Phase diagram and dynamics," The Journal of Chemical Physics **147**, 144903 (2017).
[16]T. Curk and E. Luijten, "Charge regulation effects in nanoparticle self-assembly," Phys. Rev. Lett. **126**, 138003 (2021).
[17]H. Wennerström, E. V. Estrada, J. Danielsson, and M. Oliveberg, "Colloidal stability of the living cell," Proceedings of the National Academy of Sciences **117**, 10113–10121 (2020).
[18]S. Lindsay, "Conformational flexibility in dna: Ion mediated interactions and the shape of genes," Journal of Molecular Liquids **41**, 315–325 (1989).
[19]M. Hernando-Pérez, A. X. Cartagena-Rivera, A. Lošdorfer Božič, P. J. P. Carrillo, C. San Martín, M. G. Mateu, A. Raman, R. Podgornik, and P. J. de Pablo, "Quantitative nanoscale electrostatics of viruses," Nanoscale **7**, 17289–17298 (2015).
[20]R. Kusters, H.-K. Lin, R. Zandi, I. Tsvetkova, B. Dragnea, and P. van der Schoot, "Role of charge regulation and size polydispersity in nanoparticle encapsulation by viral coat proteins," The Journal of Physical Chemistry B **119**, 1869–1880 (2015).
[21]Y. Dong, S. Li, and R. Zandi, "Effect of the charge distribution of virus coat proteins on the length of packaged rnas," Phys. Rev. E **102**, 062423 (2020).
[22]A. P. dos Santos, A. Bakhshandeh, A. Diehl, and Y. Levin, "Adsorption isotherms of charged nanoparticles," Soft Matter **12**, 8528–8533 (2016).
[23]B.-Y. Ha and D. Thirumalai, "Persistence length of flexible polyelectrolyte chains," The Journal of Chemical Physics **110**, 7533–7541 (1999).
[24]M. Rubinstein and G. A. Papoian, "Polyelectrolytes in biology and soft matter," Soft Matter **8**, 9265–9267 (2012).
[25]Y. Zheng, C. Lin, J.-S. Zhang, and Z.-J. Tan, "Ion-mediated interactions between like-charged polyelectrolytes with bending flexibility," Scientific Reports **10**, 21586 (2020).
[26]M. F. Perutz, "Electrostatic effects in proteins," Science **201**, 1187–1191 (1978).
[27]M. T. Neves-Petersen and S. B. Petersen, "Protein electrostatics: A review of the equations and methods used to model electrostatic equations in biomolecules – applications in biotechnology," (Elsevier, 2003) pp. 315–395.
[28]T. Simonson, "Electrostatics and dynamics of proteins," Reports on Progress in Physics **66**, 737 (2003).
[29]M. T. Neves-Petersen and S. B. Petersen, "Protein electrostatics: A review of the equations and methods used to model electrostatic equations in biomolecules – applications in biotechnology," (Elsevier, 2003) pp. 315–395.
[30]M. V. Fedorov and A. A. Kornyshev, "Ionic liquids at electrified interfaces," Chemical Reviews **114**, 2978–3036 (2014).
[31]P. Simon and Y. Gogotsi, "Perspectives for electrochemical capacitors and related devices," Nature Materials **19**, 1151–1163 (2020).
[32]J. Wu, "Understanding the electric double-layer structure, capacitance, and charging dynamics," Chemical Reviews **122**, 10821–10859 (2022).
[33]R. van Roij, "Defying gravity with entropy and electrostatics: sedimentation of charged colloids," Journal of Physics: Condensed Matter **15**, S3569 (2003).
[34]A. P. Philipse, "Remarks on the donnan condenser in the sedimentation–diffusion equilibrium of charged colloids," Journal of Physics: Condensed Matter **16**, S4051 (2004).
[35]A. Torres, A. Cuetos, M. Dijkstra, and R. v. Roij, "Sedimentation of charged colloids: The primitive model and the effective one-component approach," Phys. Rev. E **75**, 041405 (2007).
[36]M. Quesada-Pérez, J. Callejas-Fernández, and R. Hidalgo-Alvarez, "Interaction potentials, structural ordering and effective charges in dispersions of charged colloidal particles," Advances in colloid and interface science **95**, 295–315 (2002).
[37]A. Fernandez-Nieves, A. Fernandez-Barbero, F. de Las Nieves, and B. Vincent, "Ionic correlations in highly charge-asymmetric colloidal liquids," The Journal of chemical physics **123** (2005).
[38]A. Karnieli, T. Markovich, and D. Andelman, "Surface pressure of charged colloids at the air/water interface," Langmuir **34**, 13322–13332 (2018).
[39]A. Bakhshandeh, "Theoretical investigation of a polarizable colloid in the salt medium," Chemical Physics **513**, 195–200 (2018).
[40]D. A. Walker, B. Kowalczyk, M. O. de la Cruz, and B. A. Grzybowski, "Electrostatics at the nanoscale," Nanoscale **3**, 1316–1344 (2011).
[41]Y. Levin, "Polarizable ions at interfaces," Phys. Rev. Lett. **102**, 147803 (2009).
[42]Y. Levin, A. P. dos Santos, and A. Diehl, "Ions at the air-water interface: An end to a hundred-year-old mystery?" Phys. Rev. Lett. **103**, 257802 (2009).
[43]J.-P. Hansen and H. Löwen, "Effective interactions between electric double layers," Annual Review of Physical Chemistry **51**, 209–242 (2000).
[44]R. van Roij, "Electrostatics in liquids: From electrolytes and suspensions towards emulsions and patchy surfaces," Physica A: Statistical Mechanics and its Applications **389**, 4317–4331 (2010).
[45]V. Dahirel, M. Jardat, J. F. Dufrêche, and P. Turq, "Ion-mediated interactions between charged and neutral nanoparticles," Phys. Chem. Chem. Phys. **10**, 5147–5155 (2008).
[46]Y. Avni, D. Andelman, and R. Podgornik, "Charge regulation with fixed and mobile charged macromolecules," Current Opinion in Electrochemistry **13**, 70–77 (2019).
[47]J. Landsgesell, L. Nová, O. Rud, F. Uhlík, D. Sean, P. Hebbeker, C. Holm, and P. Košovan, "Simulations of ionization equilibria in weak polyelectrolyte solutions and gels," Soft Matter **15**, 1155–1185 (2019).
[48]M. Lund and B. Jönsson, "Charge regulation in biomolecular solution," Quarterly Reviews of Biophysics **46**, 265–281 (2013).
[49]J. G. Kirkwood and F. H. Westheimer, "The Electrostatic Influence of Substituents on the Dissociation Constants of Organic Acids. I," The Journal of Chemical Physics **6**, 506–512 (1938).
[50]F. H. Westheimer and J. G. Kirkwood, "The electrostatic influence of substituents on the dissociation constants of organic acids. ii," The Journal of Chemical Physics **6**, 513–517 (1938).

[51]J. G. Kirkwood and J. B. Shumaker, "Forces between protein molecules in solution arising from fluctuations in proton charge and configuration*," Proceedings of the National Academy of Sciences **38**, 863–871 (1952).
[52]C. Tanford and J. G. Kirkwood, "Theory of protein titration curves. i. general equations for impenetrable spheres," Journal of the American Chemical Society **79**, 5333–5339 (1957).
[53]C. Tanford, "Theory of protein titration curves. ii. calculations for simple models at low ionic strength," Journal of the American Chemical Society **79**, 5340–5347 (1957).
[54]C. Tanford and R. Roxby, "Interpretation of protein titration curves. application to lysozyme," Biochemistry **11**, 2192–2198 (1972).
[55]B. W. Ninham and V. Parsegian, "Electrostatic potential between surfaces bearing ionizable groups in ionic equilibrium with physiologic saline solution," Journal of Theoretical Biology **31**, 405–428 (1971).
[56]M. Lund and B. Jönsson, "On the charge regulation of proteins," Biochemistry **44**, 5722–5727 (2005).
[57]D. C. Prieve and E. Ruckenstein, "The surface potential of and double-layer interaction force between surfaces characterized by multiple ionizable groups," Journal of Theoretical Biology **56**, 205–228 (1976).
[58]S. H. Behrens and M. Borkovec, "Exact poisson-boltzmann solution for the interaction of dissimilar charge-regulating surfaces," Phys. Rev. E **60**, 7040–7048 (1999).
[59]G. S. Longo, M. Olvera de la Cruz, and I. Szleifer, "Molecular theory of weak polyelectrolyte gels: The role of ph and salt concentration," Macromolecules **44**, 147–158 (2011).
[60]I. Popa, P. Sinha, M. Finessi, P. Maroni, G. Papastavrou, and M. Borkovec, "Importance of charge regulation in attractive double-layer forces between dissimilar surfaces," Phys. Rev. Lett. **104**, 228301 (2010).
[61]A. Bakhshandeh, D. Frydel, and Y. Levin, "Charge regulation of colloidal particles in aqueous solutions," Phys. Chem. Chem. Phys. **22**, 24712–24728 (2020).
[62]E. Lee, T.-S. Tong, M.-H. Chih, and J.-P. Hsu, "Sedimentation of concentrated spherical particles with a charge-regulated surface," Journal of Colloid and Interface Science **251**, 109–119 (2002).
[63]P. M. Biesheuvel, "Evidence for charge regulation in the sedimentation of charged colloids," Journal of Physics: Condensed Matter **16**, L499 (2004).
[64]A. Seiphoori, A. Gunn, S. Kosgodagan Acharige, P. E. Arratia, and D. J. Jerolmack, "Tuning sedimentation through surface charge and particle shape," Geophysical Research Letters **48**, e2020GL091251 (2021).
[65]F. Fogolari, A. Brigo, and H. Molinari, "The poisson–boltzmann equation for biomolecular electrostatics: a tool for structural biology," Journal of Molecular Recognition **15**, 377–392 (2002).
[66]M. Sato, A. Harata, Y. Hatano, T. Ogawa, T. Kaieda, K. Ohmukai, and H. Kawazumi, "Acid-base equilibrium constants and distribution coefficients of aminopyrene between the surface and bulk of liquid water as studied by a laser two-photon ionization technique," The Journal of Physical Chemistry B **108**, 12111–12115 (2004).
[67]G. Oliviero, S. Federici, P. Colombi, and P. Bergese, "On the difference of equilibrium constants of dna hybridization in bulk solution and at the solid-solution interface," Journal of Molecular Recognition **24**, 182–187 (2011).
[68]A. Bakhshandeh, D. Frydel, A. Diehl, and Y. Levin, "Charge regulation of colloidal particles: Theory and simulations," Phys. Rev. Lett. **123**, 208004 (2019).
[69]R. Messina, C. Holm, and K. Kremer, "Effect of colloidal charge discretization in the primitive model," The European Physical Journal E **4**, 363–370 (2001).
[70]A. Bakhshandeh, A. P. dos Santos, and Y. Levin, "Interaction between charge-regulated metal nanoparticles in an electrolyte solution," The Journal of Physical Chemistry B **124**, 11762–11770 (2020).
[71]D. A. Gomez, D. Frydel, and Y. Levin, "Lattice-gas model of a charge regulated planar surface," The Journal of Chemical Physics **154**, 074706 (2021).
[72]M. Muthukumar, J. Hua, and A. Kundagrami, "Charge regularization in phase separating polyelectrolyte solutions," The Journal of Chemical Physics **132**, 084901 (2010).
[73]P. M. Blanco, S. Madurga, F. Mas, and J. L. Garcés, "Effect of charge regulation and conformational equilibria in the stretching properties of weak polyelectrolytes," Macromolecules **52**, 8017–8031 (2019).
[74]M. Stornes, P. M. Blanco, and R. S. Dias, "Polyelectrolyte-nanoparticle mutual charge regulation and its influence on their complexation," Colloids and Surfaces A: Physicochemical and Engineering Aspects **628**, 127258 (2021).
[75]A. Salehi and R. G. Larson, "A molecular thermodynamic model of complexation in mixtures of oppositely charged polyelectrolytes with explicit account of charge association/dissociation," Macromolecules **49**, 9706–9719 (2016).
[76]T. Curk, J. Yuan, and E. Luijten, "Accelerated simulation method for charge regulation effects," The Journal of Chemical Physics **156**, 044122 (2022).
[77]Y. Levin and A. Bakhshandeh, "A new method for reactive constant pH simulations," The Journal of Chemical Physics **159**, 111101 (2023).
[78]A. Y. Toukmaji and J. A. Board, "Ewald summation techniques in perspective: a survey," Computer Physics Communications **95**, 73–92 (1996).
[79]A. P. dos Santos, M. Girotto, and Y. Levin, "Simulations of Coulomb systems with slab geometry using an efficient 3D Ewald summation method," The Journal of Chemical Physics **144**, 144103 (2016).
[80]A. P. dos Santos, M. Girotto, and Y. Levin, "Simulations of coulomb systems confined by polarizable surfaces using periodic green functions," The Journal of Chemical Physics **147**, 184105 (2017).
[81]M. Girotto, A. P. dos Santos, and Y. Levin, "Simulations of ionic liquids confined by metal electrodes using periodic green functions," The Journal of Chemical Physics **147**, 074109 (2017).
[82]S. Stenberg and B. Stenqvist, "An exact ewald summation method in theory and practice," The Journal of Physical Chemistry A **124**, 3943–3946 (2020).
[83]M. Girotto, T. Colla, A. P. dos Santos, and Y. Levin, "Lattice model of an ionic liquid at an electrified interface," The Journal of Physical Chemistry B **121**, 6408–6415 (2017).
[84]M. Girotto, A. P. dos Santos, and Y. Levin, "Simulations of ionic liquids confined by metal electrodes using periodic Green functions," The Journal of Chemical Physics **147**, 074109 (2017).
[85]A. Z. P. J. Karl Johnson and K. E. Gubbins, "Reactive canonical monte carlo," Molecular Physics **81**, 717–733 (1994).
[86]T. W. Rosch and E. J. Maginn, "Reaction ensemble monte carlo simulation of complex molecular systems," Journal of Chemical Theory and Computation **7**, 269–279 (2011).

[87]A. Bakhshandeh, D. Frydel, and Y. Levin, "Reactive Monte Carlo simulations for charge regulation of colloidal particles," The Journal of Chemical Physics **156**, 014108 (2022).
[88]W. R. Smith and B. Triska, "The reaction ensemble method for the computer simulation of chemical and phase equilibria. I. Theory and basic examples," The Journal of Chemical Physics **100**, 3019–3027 (1994).
[89]A. Z. P. J. Karl Johnson and K. E. Gubbins, "Reactive canonical monte carlo," Molecular Physics **81**, 717–733 (1994).
[90]Y. Levin and A. Bakhshandeh, "Comment on "simulations of ionization equilibria in weak polyelectrolyte solutions and gels" by j. landsgesell, l. nová, o. rud, f. uhlík, d. sean, p. hebbeker, c. holm and p. košovan, soft matter, 2019, 15, 1155–1185," Soft Matter **19**, 3519–3521 (2023).
[91]A. Bakhshandeh and Y. Levin, "Widom insertion method in simulations with Ewald summation," The Journal of Chemical Physics **156**, 134110 (2022).
[92]A. Bakhshandeh and Y. Levin, "Charge fluctuations in charge-regulated systems: dependence on statistical ensemble," The European Physical Journal E **46**, 65 (2023).
[93]A. Bakhshandeh and Y. Levin, "Canonical titration simulations," Phys. Chem. Chem. Phys. **25**, 32800–32806 (2023).
[94]J.-P. Hansen and I. R. McDonald, "Chapter 3 - static properties of liquids: Thermodynamics and structure," in *Theory of Simple Liquids (Fourth Edition)*, edited by J.-P. Hansen and I. R. McDonald (Academic Press, Oxford, 2013) fourth edition ed., pp. 61–104.
[95]Herein, the term "excess" is used to express inter-particle interactions beyond mean-field.
[96]Y. Levin and J. E. Flores-Mena, "Surface tension of strong electrolytes," Europhysics Letters **56**, 187 (2001).
[97]Y. Levin and A. P. dos Santos, "Ions at hydrophobic interfaces," Journal of Physics: Condensed Matter **26**, 203101 (2014).
[98]A. Bakhshandeh, D. Frydel, and Y. Levin, "Theory of charge regulation of colloidal particles in electrolyte solutions," Langmuir **38**, 13963 (2022).
[99]A. P. dos Santos, A. Diehl, and Y. Levin, "Colloidal charge renormalization in suspensions containing multivalent electrolyte," The Journal of Chemical Physics **132**, 104105 (2010).
[100]D. Henderson and L. Blum, "Some exact results and the application of the mean spherical approximation to charged hard spheres near a charged hard wall," The Journal of Chemical Physics **69**, 5441–5449 (1978).
[101]D. Henderson, L. Blum, and J. L. Lebowitz, "An exact formula for the contact value of the density profile of a system of charged hard spheres near a charged wall," Journal of Electroanalytical Chemistry and Interfacial Electrochemistry **102**, 315–319 (1979).
[102]S. L. Carnie, D. Y. C. Chan, D. J. Mitchell, and B. W. Ninham, "The structure of electrolytes at charged surfaces: The primitive model," J. Chem. Phys. **74**, 1472–1478 (1981).
[103]H. Wennerström, B. Jönsson, and P. Linse, "The cell model for polyelectrolyte systems. exact statistical mechanical relations, monte carlo simulations, and the poisson–boltzmann approximation," The Journal of Chemical Physics **76**, 4665–4670 (1982).
[104]M. Lozada-Cassou, "The force between two planar electrical double layers," J. Chem. Phys. **80**, 3344–3349 (1984).
[105]J. P. Mallarino, G. Téllez, and E. Trizac, "The contact theorem for charged fluids: from planar to curved geometries," Mol. Phys. **113**, 2409–2427 (2015).
[106]A. Bakhshandeh and Y. Levin, "Titration in canonical and grand-canonical ensembles," The Journal of Physical Chemistry B **127**, 9405–9411 (2023).
[107]A. Bakhshandeh and Y. Levin, "On the validity of constant ph simulations," Journal of Chemical Theory and Computation **20**, 1889–1896 (2024).
[108]J. D. Jackson, *Classical electrodynamics* (Third edition. New York : Wiley, 1999).